Interactions between Upper and Lower Tropospheric Gravity Waves on Squall Line Structure and Maintenance

JEROME M. SCHMIDT AND WILLIAM R. COTTON

Colorado State University, Department of Atmospheric Science, Fort Collins, Colorado

(Manuscript received 27 April 1989, in final form 15 November 1989)

ABSTRACT

Using a simplified thermodynamic sounding, and variable vertical wind shear, we investigate the role of gravity waves on the structure and propagation of a simulated two-dimensional squall line. Based on an observed squall line environment, the modeled troposphere has been divided into three distinct thermodynamic layers. These consist of an absolutely stable atmospheric boundary layer (ABL), an elevated well-mixed layer, and an upper tropospheric layer of intermediate stability. We find the mixed layer to have a dual role; it has a reduced stability and thus provides abundant buoyancy for the convective scale updrafts, and it provides an ideal layer to trap mesoβ-scale (20–200 km) wave energy generated in the stable layers. The generated waves thus have a significant and lasting impact on the simulation.

We also find this thermodynamic structure to be conducive to both strong surface wind perturbations and long-lived squall lines. Experiments that vary the vertical wind shear profile demonstrate that the most vigorous and long-lived squall lines arise with a deep layer of strong vertical wind shear. This result is dependent on the changes in the phase speed and magnitude of the stable layer waves that occur in the sheared versus nonsheared environments. Without flow, waves generated by an initial heat pulse split into symmetric leftward and rightward moving disturbances. Waves generated in the upper tropospheric stable layer are found to move relative to the lower tropospheric waves resulting in a decoupling of deep tropospheric vertical motion and a decrease in strength of the simulated system. With vertical wind shear, the magnitude of the simulated waves is enhanced and an opportunity for sustained coupling between the upper and lower waves exists. It is shown that the upper and lower tropospheric waves in a sheared environment account for many of the circulation features typically associated with two-dimensional squall lines.

A simple mechanism for the rear-to-front middle-level jet and surface wake low is also presented.

1. Introduction

One of the fundamental responses to a region of heating in a stratified fluid is the generation of internal gravity waves. In the atmosphere, gravity waves provide an effective mechanism to redistribute momentum and heat over a wide spectrum of length and time scales. We will restrict our attention here to mesoβ-scale (20–200 km) gravity waves that exhibit long lifetimes (several hours). Waves of such length and time scales have frequently been resolved in synoptic surface networks in association with severe mesoscale convective systems (MCSs) (cf. Eom 1975; Uccellini 1975; Miller and Sanders 1980; Stobie et al. 1983; Bosart and Seimon 1988; Koch et al. 1988). These studies have described wave–convective interaction in terms of MCS initiation, propagation speed, and related surface weather. Less well understood are the effects of gravity waves, generated in an environment of strong vertical wind shear, on the internal flow structures that evolve within a developing MCS. It is this aspect of wave–convective interaction that will serve as the primary focus of this paper. Our particular interests are in MCSs which exhibit squall line structure.

Some of the initial studies of gravity wave–squall line interaction were concerned with the role of gravity waves on squall line propagation and orientation to the mean flow (Hamilton and Archbold 1945; Freeman 1948; Tepper 1950; Abdullah 1954). The squall line was modeled as a hydraulic jump propagating on a thin elevated inversion separating the moist atmospheric boundary layer (ABL) from the dry ambient air aloft. Their calculations of the hydraulic jump speed appeared to give reasonable predictions for the propagation speed of observed squall lines and the low-level lift generated by the jump provided a mechanism to aid the low-level updraft required to sustain the line. This hypothesis appeared to gain popular support despite early objections by Newton (1950) who questioned whether the squall line would destroy the inversion required for the jump. He and others have proposed an alternative mechanism for squall line propagation and maintenance, namely, the production of a surface cold pool that behaves as a pseudo–cold front. The interaction between the surface cold pool and the low-level vertical wind shear has since formed

Corresponding author address: Jerome M. Schmidt, Department of Atmospheric Science, Colorado State University, Fort Collins, CO 80523.

a basis for more recent theoretical work (Thorpe et al. 1982; Rotunno et al. 1988).

More recent studies have cast wave–convective interaction in terms of two- and three-dimensional linear theory (Emanuel 1982; Bolton 1984; Raymond 1984, 1986; Lin and Smith 1986; Orlanski and Ross 1986; Lin and Li 1988; Nicholls 1989). The waves are studied in simplified environments consisting of one or more layers of constant static stability and constant vertical wind shear so that analytical solutions could be obtained. Despite the simplifications, these studies have shown that many squall line circulation features, such as the surface pressure distribution, broad regions of mesoscale inflow and outflow within the middle and upper troposphere, and the updraft structure are well represented within the linearized framework.

A general concern of the linear theory is to find growing wave modes of the proper time scales and phase speeds generally observed for squall lines (Nehrkorn 1986). Part of the problem stems from the tendency for gravity waves to propagate energy vertically. Without additional energy input or a mechanism to reflect the wave energy, a propagating wave would rapidly decrease in amplitude before traveling horizontally for even a few cycles (Lindzen and Tung 1976).

On occasion a layer in the atmosphere is formed, referred to as a wave duct, where horizontal propagation may proceed without energy loss. An example of upper tropospheric wave ducting was discussed by Tripoli and Cotton (1989a,b). In their numerical study, gravity waves were trapped in and beneath the upper tropospheric cirrus cloud shield associated with a simulated MCS. The wave duct resulted from radiative cooling at cloud top, which produced a rapid decrease in the Scorer parameter just above the cloud top. Consequently, gravity waves emitted from the convective region of the MCS had a lasting effect on the simulated flow fields within the stratiform region of the system.

Atmospheric conditions conducive to ducted mesoβ-scale gravity waves within the lower troposphere were described by Lindzen and Tung (1976). They showed the most efficient wave ducts occur when a layer of low static stability, containing a steering level (i.e., where the environmental flow speed equals the wave phase speed) overlies a deep, stable ABL (referred to as the ducting layer). It seems reasonable to assume, in that these conditions may also approximate the environment of many nocturnal or overriding frontal squall lines (Porter et al. 1955; Duhdia et al. 1987), that squall lines and ducted waves could coexist. The stable layer required for the wave duct may at first seem to inhibit squall line development but, in fact, it appears as a common feature in many strong-to-severe squall lines (Brunk 1949; Tepper 1950; Porter et al. 1955; Carbone 1982; Johns and Hirt 1987; Branick et al. 1988; Schmidt and Cotton 1989).

The purpose of this paper is to examine the role of gravity waves, ducted or otherwise, on the propagation and internal flow characteristics of a simulated squall line. In particular we examine the sensitivity of the wave and squall line structure to changes in the modeled vertical wind shear. The simulations are based on an observed squall line which produced severe surface wind gusts in excess of 30 m s^{-1} (Schmidt and Cotton 1989). One of the characteristic thermodynamic features of the presquall environment was the presence of a deep, absolutely stable ABL. We find this thermodynamic characteristic to be particularly conducive to strong surface wind perturbations and long-lived squall lines. Thus, the results may have implications to long-lived damaging wind storms, known as derechos, which often form on the stable side of synoptic scale frontal boundaries (Johns and Hirt 1987).

2. Methodology

a. Model description

The numerical model used to perform the simulations is a nonhydrostatic version of the Colorado State University Regional Atmospheric Mesoscale Modeling System (RAMS) [a more complete description of this model may be found in Tripoli (1986) and Nicholls (1987)]. The model consists of a set of nonhydrostatic compressible dynamic equations, a thermodynamic equation, and a set of microphysical equations that account for interactions between all phases of water. The Klemp–Wilhelmson (1978) radiation condition is applied on the lateral boundaries and, to prevent unwanted reflection of wave energy from the top boundary, an absorbing layer 5 km thick was placed at the top of the model domain.

b. Domain size and resolution

The choice of domain size and resolution reflects a desire to show the affects of gravity waves on both the convective-scale and mesoscale circulations with a developing squall line. Because the gravity waves traveled quickly and varied in horizontal scale, the simulations required a large domain with relatively fine horizontal resolution. For these reasons, a two-dimensional x–z domain of 400 × 23 km was selected for the initial simulations. The domain has a horizontal grid spacing of 2 km, while a stretched grid varies the vertical resolution from 300 m in the ABL to constant value of 500 m aloft. Tests made with a finer horizontal resolution (1 km) showed a nearly identical development of the squall line as the coarse resolution simulations. The coarser grid was thus chosen to keep the computer cost at a minimum.

c. Model initialization

The thermodynamic and vertical wind shear profiles used to initialize the model (Fig. 1) were based on a composite sounding derived from aircraft and rawinsonde data acquired from the CCOPE field network

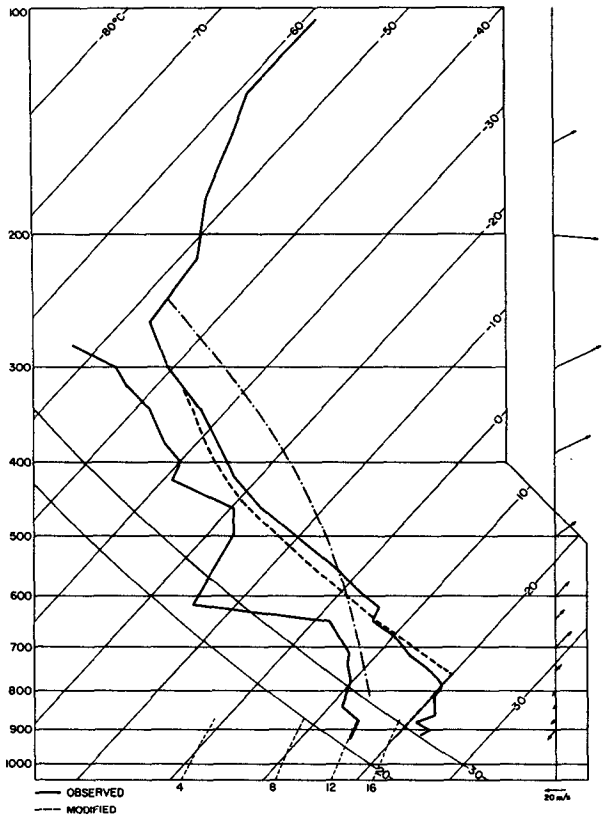

FIG. 1. Environmental sounding of temperature and dewpoint temperature of the presquall environment from Knowlton, Montana on 2 August 1981 (solid lines) used to initialize the control experiment. The sounding was modified below 60 kPa with aircraft soundings taken immediately ahead of the squall line. The thin dashed line represents the simplifications made to the observed temperature profile used to initialize experiments S0–S3 and FS2. Parcel ascent based on the observed environment is shown as the dot–dash line.

(located in the High Plains region of southeastern Montana) for the presquall environment of 2 August 1981. [A more complete mesoscale analyses and storm description for this day can be found in Miller et al. (1988) and Schmidt and Cotton (1989).] The sounding revealed three distinct thermodynamic layers within the troposphere consisting of: 1) a moist, but stable ABL approximately 1200 m deep, 2) a deep, nearly dry adiabatic layer to 45 kPa, and 3) an upper tropospheric stable layer of intermediate stability. The temperature profile within the stratosphere gradually became isothermal and, for lack of a better choice, we simply extend this profile beyond the sounding termination level (5 kPa) to the model top.

The sounding was also characterized by deep vertical wind shear. The flow veered with height from an east-northeasterly direction within the stable ABL, to a westerly component aloft. The u-component of the flow, which will be used to initialize the model, had a surface value of -10 m s^{-1} and a peak speed of 40 m s^{-1} at the tropopause (9.2 km AGL) giving a tropospheric shear value of 5.4×10^{-3} s^{-1}. The wind in the stratosphere weakened to a value of 10 m s^{-1} near 5 kPa and, above that point, was set to a constant value of zero.

The model was initialized with the above sounding using a warm bubble technique. This technique was chosen in lieu of a surface cold pool initialization because it was of some interest to determine the effects of the stable ABL on the cold pool development. The bubble was derived by adding a tendency to the initially horizontally homogeneous fields of potential temperature and mixing ratio. The tendencies were applied for the first 600 s of the simulation and resulted in a potential temperature perturbation (θ') of 2°C and a mixing ratio perturbation (q') of 2 g kg^{-1} at the center of a bubble 12 km across and 2 km deep. To provide a smooth transition to the undisturbed environment, the tendency was reduced outward from the center of the bubble to a value of zero at the edge of the bubble.

d. Experimental design

Table 1 lists the features of the numerical experiments described in this paper. Our approach is to first present the squall line simulation based on the composite sounding shown in Fig. 1 (referred to as the control in Table 1). Additional experiments are then presented that use simplified thermodynamic and vertical shear profiles (labeled S0–S3 in Table 1). Our motivation for using the simplified sounding (shown as the dashed line in Fig. 1) is to eliminate the smaller-

TABLE 1. Experimental design showing the magnitude of the vertical wind shear within the troposphere and the static stability of the three tropospheric layers evident in the sounding of Fig. 1. The Brunt–Väisälä frequencies of the lower (N_1), middle (N_2), and upper tropospheric (N_3) layer of the modified sounding are provided for later reference.

Experiment	Three layer static stability $\left(g/\theta \frac{\partial\theta}{\partial Z}\right)^{1/2}$	Mean tropospheric vertical wind shear	Horizontal resolution
Control	Variable	5.4×10^{-3} s^{-1}	2 km
S0	$N_1 = 1.6 \times 10^{-2}$ s^{-1} $N_2 = 3.4 \times 10^{-3}$ s^{-1} $N_3 = 1 \times 10^{-2}$ s^{-1}	0	2 km
S1	$N_1 = 1.6 \times 10^{-2}$ s^{-1} $N_2 = 3.4 \times 10^{-3}$ s^{-1} $N_3 = 1 \times 10^{-2}$ s^{-1}	2.5×10^{-3} s^{-1}	2 km
S2	$N_1 = 1.6 \times 10^{-2}$ s^{-1} $N_2 = 3.4 \times 10^{-3}$ s^{-1} $N_3 = 1 \times 10^{-2}$ s^{-1}	5.0×10^{-3} s^{-1}	2 km
S3	$N_1 = 1.6 \times 10^{-2}$ s^{-1} $N_2 = 3.4 \times 10^{-3}$ s^{-1} $N_3 = 1 \times 10^{-2}$ s^{-1}	6.7×10^{-3} s^{-1}, $z < 3$ km 0, $z > 3$ km	2 km
FS2	$N_1 = 1.6 \times 10^{-2}$ s^{-1} $N_2 = 3.4 \times 10^{-3}$ s^{-1} $N_3 = 1 \times 10^{-2}$ s^{-1}	5.0×10^{-3} s^{-1}	1 km

scale temperature fluctuations evident in the composite sounding, while at the same time retaining the three thermodynamically distinct tropospheric layers. We will show that the modified thermodynamic profile does not significantly alter the basic flow structures that evolve in the model, but it will simplify the analysis of the gravity waves to be presented in later sections. The simplified thermodynamic structure should also lend itself to analytical solutions as well, but these are not attempted here.

The idealized three-layer thermodynamic profile, though based on a single observation, may well represent the thermodynamic structure of the troposphere in a variety of conditions. The stable ABL can arise from nocturnal cooling, shallow fronts, or, as in the present case, previous convection. The overlying layer of low static stability may result from differential temperature advection near synoptic scale cyclones (Newton 1966; Carr and Millard 1985) or, as may often be the case in the western United States, the eastward advection of the daytime mountain ABL over the Central Plains (Benjamin and Carlson 1986). The depth of the elevated mixed layer must be limited to some extent, thus giving rise on occasion to a third layer of some intermediate stability within the upper troposphere. The primary differences from case to case will be the depth of the respective layers and the structure of the vertical wind shear profile.

In this paper the thermodynamic profiles are fixed as we examine the model response to changes in the vertical wind shear profile. In experiment S0 the initial flow was set to zero everywhere within the domain. This experiment is particularly useful in showing the structure of the primary gravity waves resulting from the initial perturbation. We then reintroduce shear to the model in experiments S1, S2 and FS2 by specifying a linear shear profile over the depth of the troposphere. In an attempt to replicate the observed wind profile of Fig. 1, the u-component in experiment S2 ranged from a surface minimum of -10 m s^{-1} to a maximum of 40 m s^{-1} at 10 km AGL. The u-component within the stratosphere is reduced linearly to zero by 15 km. The u-component of experiment S1 was simply set to half the value used in experiment S2 at each level within the domain. The u-component in experiment S3 was identical to S2 up to a level of 3 km and set to a constant value of 10 m s^{-1} above that point.

The control experiment and experiments S0–S3 were initialized from $t = 0$ and integrated for 14 400 s. Thus the present results are relevant only to the initial stages of squall line development.

3. Experimental results

a. Control run

The modeled fields of perturbation Exner function (π'), potential temperature (θ'), horizontal flow (u') (obtained as departures from the initial state), vertical motion (w), and θ are shown for the control run at 7200 s in Fig. 2. Though early in the simulation the perturbation flow at this time resembles the 2-D squall line circulation of Newton (1950), Thorpe et al. (1982), and Smull and Houze (1987). The initial perturbation has produced a narrow, convective-scale updraft region of 9 m s^{-1} exhibiting a slight upshear tilt (Fig. 2a). Deep layers of upper-level outflow and middle-level inflow are evident on either flank of the primary updraft (Fig. 2b).

The perturbation fields within the lower portion of the primary updraft are responding to a low-level gravity wave that formed in the stable surface layer. The counterclockwise perturbation flow about the wave[1] formed the convective-scale updraft/downdraft couplet near $x = 25$ (Fig. 2a) and surface u' values of 22 m s^{-1}. The strong positive u' was a result of the upward displacement of the theta surfaces (Fig. 2a), which produced a cooling of -4°C and a pressure rise of 0.8 J kg^{-1} K^{-1}. The wave movement, from left to right at 19 m s^{-1}, accounted for the rapid speed of the simulated squall line (also 19 m s^{-1}) and closely matches the 21 m s^{-1} movement of the observed squall line reported by Schmidt and Cotton (1989).

b. Experiments using the idealized sounding

For the remainder of the paper we consider the flow structures obtained using the modified thermodynamic and vertical shear profiles listed in Table 1 for experiments S0–S3. Our goal is to replicate the general flow features obtained in the control run as we systematically increase the magnitude of the vertical wind shear from zero (experiment S0) to the magnitude observed in the control (experiment S2). The following four subsections also illustrate the structure of the simulated gravity waves generated in the upper and lower tropospheric stable layers, and the role of wind shear in changing the phase speed and magnitude of these waves. It will become apparent that the structure and relative vertical alignment of the gravity waves in the sheared environment account for many of the flow structures obtained in the control run. The structural changes induced by the vertical wind shear are summarized with a conceptual model at the end of this section.

1) EXPERIMENT S0 (ZERO FLOW)

The zero flow experiment (S0) clearly shows the field of gravity waves generated as the initial bubble accelerated upward through the various layers within the troposphere (Fig. 3). The gravity waves, in the form of single waves of elevation or depression, have produced large perturbations within the upper and lower tropospheric stable layers and a relatively weak response within the well-mixed layer. Except for the field

[1] Though a closed circulation is suggested by the perturbation velocity fields, the wave relative flow remains front-to-rear at all levels.

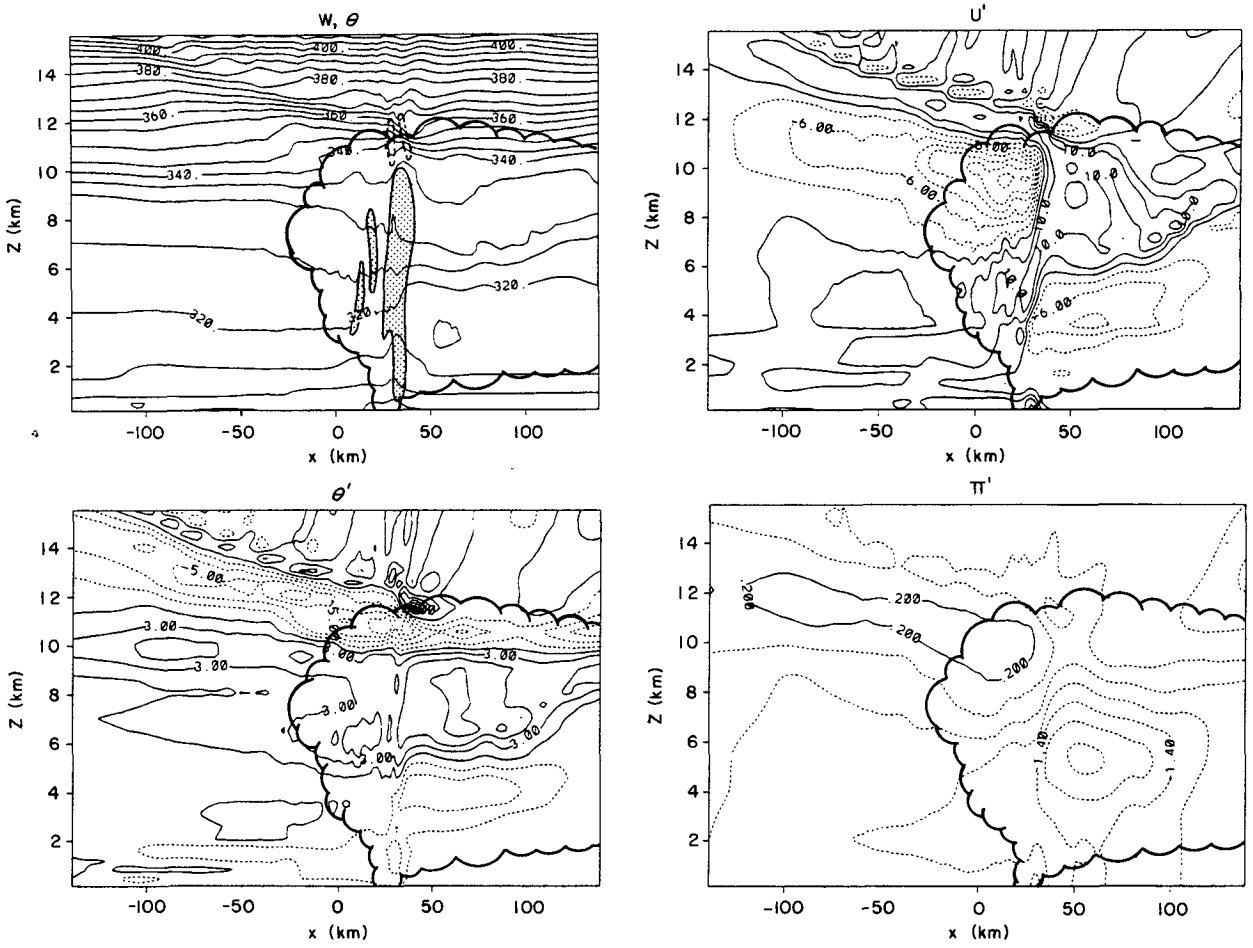

FIG. 2. Vertical x–z cross-sections of the control experiment at 7200 s. (a) Potential temperature (θ) contoured every 5 K and vertical motion (w). Updrafts greater than 1 m s^{-1} are shaded. Downdraft less than -1 m s^{-1} are denoted by the dashed lines. (b) perturbation zonal velocity u' every 4 m s^{-1}, (c) perturbation potential temperature θ' (every 2 K), (d) perturbation Exner function contoured every 0.4 J kg^{-1} K^{-1}. Scalloped line in each panel denotes the cloud boundary. Note that only a portion of the entire domain is shown.

of u', the wave generated perturbations had left/right symmetry about a vertical line through the region of initial heating (applied near $x = 0$). The asymmetry in the u' field (a change in sign) reflects the effects of mass continuity as the horizontal flow responds to the vertical motion associated with the displacement of the isentropes during the wave passage. The wave induced circulations may thus be regarded as horizontal vorticity couplets of opposite sign moving outward from the region of initial heating.

A significant difference between the upper and lower waves is their speed of propagation away from the heat source. The lower tropospheric waves (labeled LRW and LLW[2]) had a phase speed of ± 15 m s^{-1}, roughly half the value for the corresponding upper level waves. The lower tropospheric waves were a direct result of the displacement in the isentropic surfaces generated by the initial heating applied near the top of the stable layer. Because of this, several simulations were performed to test the sensitivity of their horizontal wavelength (approximately 10 km at half amplitude) and phase speed to the initial bubble size. We found that simulations initialized with bubbles ranging between 5 and 20 km in length produced only slight departures from the values of wavelength and phase speed listed above. This suggests that these parameters were selected by other means, a topic which we defer until section 4.

The URW and ULW were generated as the initial bubble, aided by additional latent heat release, accelerated upward through the well-mixed layer, and penetrated the upper tropospheric stable layer. The URW and ULW had a much larger horizontal and vertical wavelength than their lower tropospheric counterparts.

[2] Because the perturbation quantities associated with these waves are strongest within the stable ABL, we will for convenience refer to the lower right moving waves as LRW and the lower left moving waves as the LLW. Similar labeling will be used for the upper right (URW) and upper left (ULW) waves.

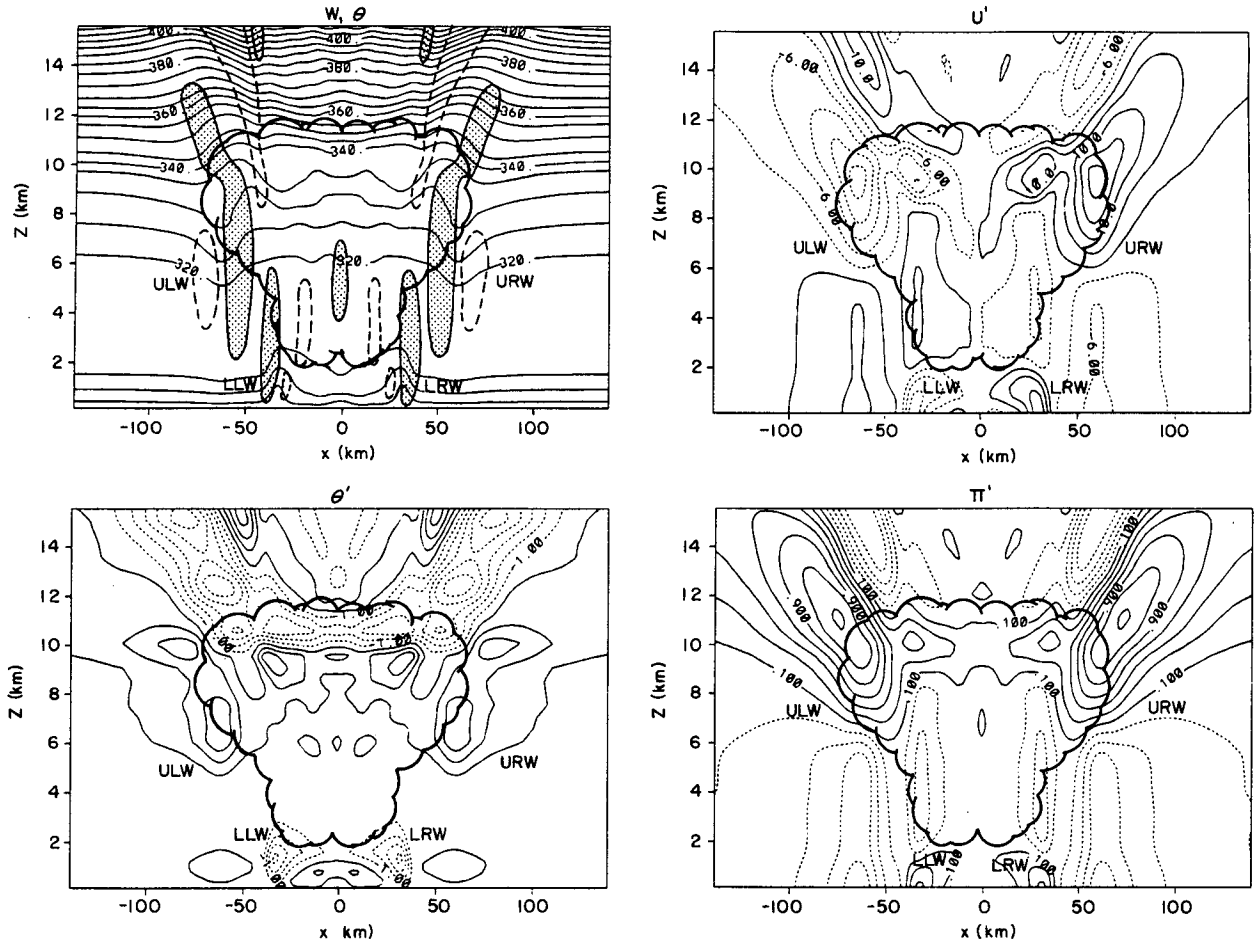

FIG. 3. As in Fig. 2, except for the zero initial flow experiment (S0) at 3600 s. The labels ULW, URW, LLW, and LRW denote the primary waves discussed in the text. Note that the contour interval in (d) has been changed to 0.2 J kg^{-1} K^{-1}.

An inspection of the u' (Fig. 3b) and π' (Fig. 3d) fields suggest a vertical wavelength within the troposphere of roughly twice the tropopause depth for the ULW and URW. The result in the pressure field is a large high centered near the tropopause and a deep layer of low pressure extending beneath the axis of warm air generated by the downward displacement of the isentropes. Above the tropopause, the high pressure axis became inclined from the vertical and the vertical wavelength shortened as the upward traveling waves adjusted to the higher static stability within the stratosphere. The other field variables were likewise inclined and their relation to the pressure field may be inferred from the polarization equations for plane internal geometry waves. The phase lines within the stratosphere propagated downward with time suggesting an upward propagation of wave energy and an eventual loss in amplitude for the ULW and URW.

An inspection of Fig. 4 shows that experiment S0, like the control experiment, was unable to sustain a vigorous updraft. As recently shown in other studies, the development of a deep convective updraft may depend on the relative alignment of the upper and lower level waves at a given time (Orlanski and Ross 1986; Baliji and Clark 1988). This may be seen in Fig. 5, which shows a time sequence of the vertical motion field from experiment S0. In Fig. 5a the updrafts of the URW and LRW were vertically aligned resulting in an upright updraft through the entire depth of the troposphere. Because the URW moved faster than the LRW, this relationship was short lived and by 4800 s the updraft of the URW had completely decoupled from the LRW (Fig. 5b). Without subsequent pulsing near the initial heat source, further development in the far field would cease at this point because neither updraft, acting alone, was able to initiate new growth in this stable environment. This simulation is thus characterized by periodic burst of deep development as subsequent pulses within the upper troposphere temporarily aligned with the slower moving lower tropospheric waves.

The wave structure in this simple experiment, though unremarkable, provides useful insight into the more complex flow structures obtained in the control

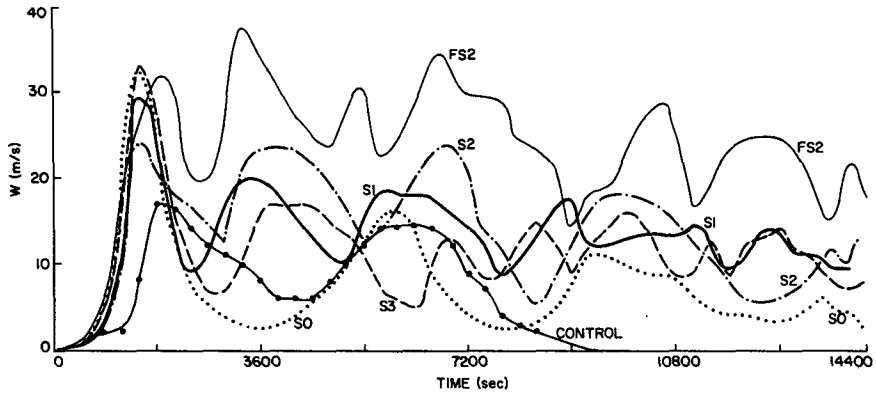

FIG. 4. Time plot of the maximum vertical motion for the experiments listed in Table 1. The line labeled FS2 represents the results of rerunning experiment S2 with a 1 km horizontal resolution.

simulation. Note in particular that the asymmetry in u' for the upper and lower waves (Fig. 3b) has produced the basic structure of the horizontal flow observed on either flank of the squall line in the control run (Fig. 2b); i.e., deep layers of negative/positive u' in the upper tropospheric stable layer and a return flow within the well-mixed layer. Note also that there is a close correspondence in the magnitude of the upper tropospheric perturbations in u and θ between the two experiments (compare Figs. 2b,c and 3b,c). These crude structural similarities suggest that the flow structures simulated in the control experiment were strongly

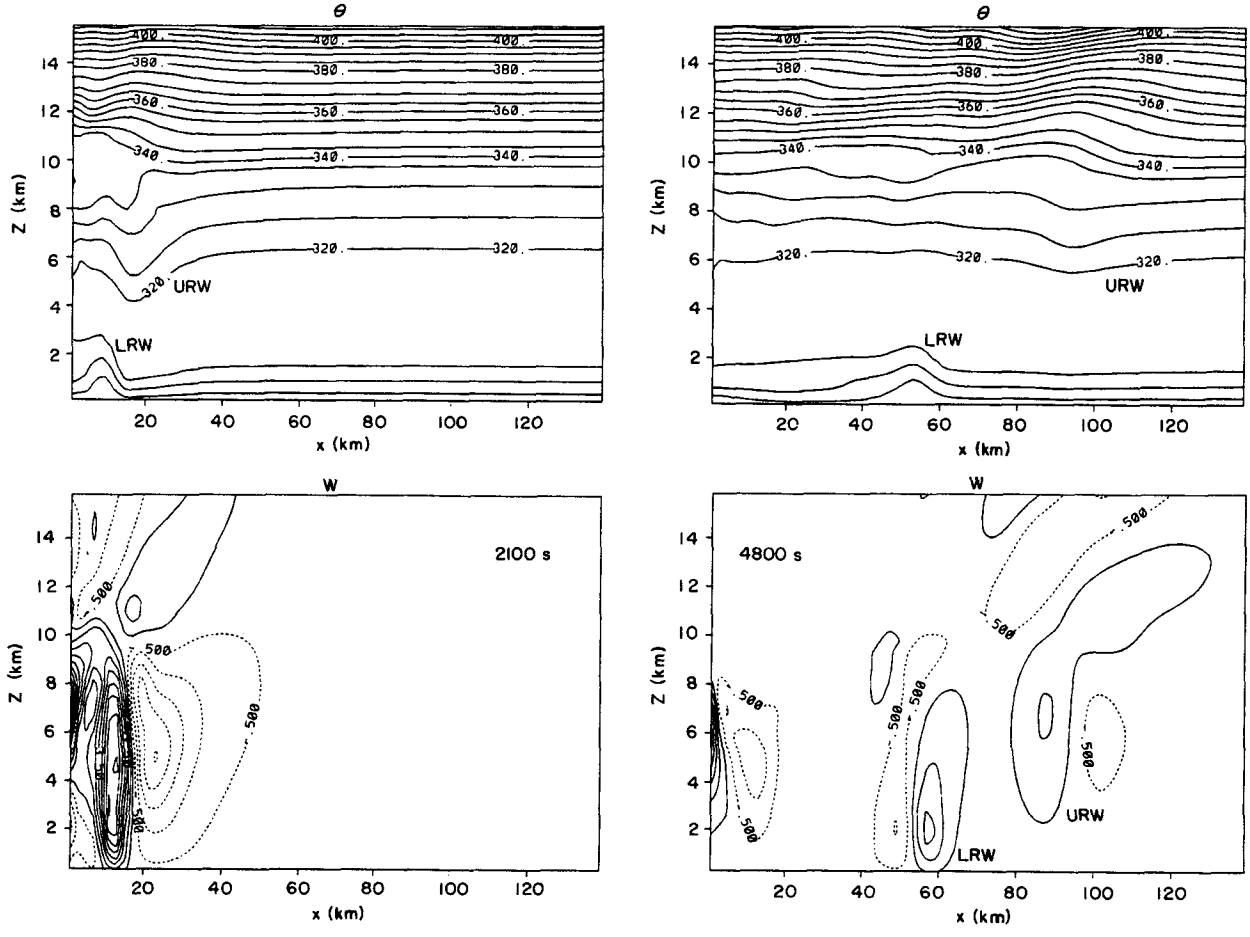

FIG. 5. Vertical x–z cross section of θ and w for experiment S0 at (a) 2100 s, and (b) 4800 s. The value of w is contoured every 1 m s^{-1}.

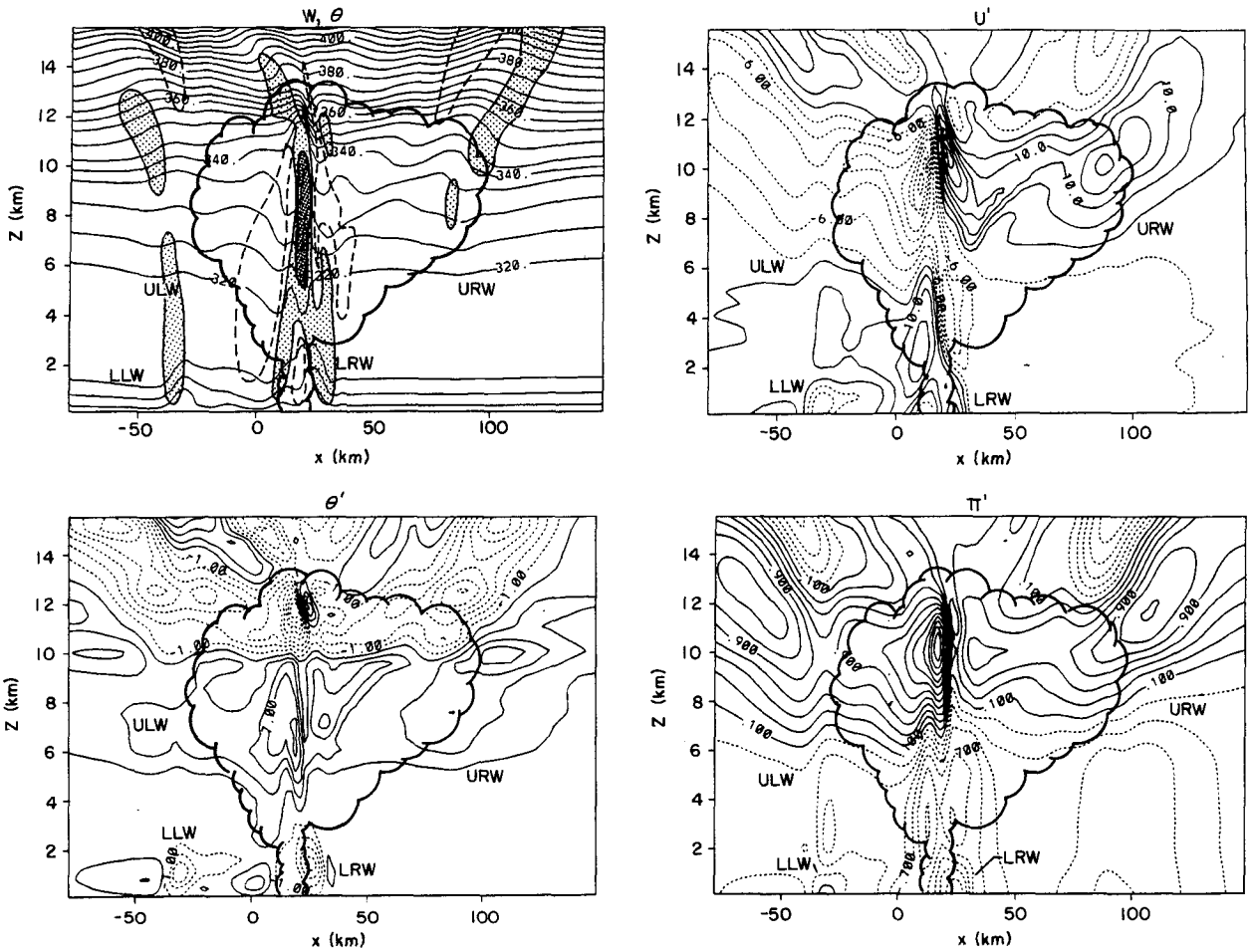

FIG. 6. As in Fig. 3 except for experiment S1 (weak shear) at 3600 s. Darker shading denotes updraft in excess of 10 m s^{-1}.

modulated by the gravity waves. This relationship is pursued further in the following subsections as vertical wind shear is reintroduced into the simulations.

2) WEAK SHEAR EXPERIMENT (S1)

The addition of shear had two primary effects on the simple symmetry obtained in experiment S0 (Fig. 6). First, the left-to-right flow across the domain induced a Doppler shift in the wave phase speed in both upper and lower layers. Because the flow was stronger aloft, the upper level waves experienced a greater shift (15 vs 5 m s^{-1}) and were thus shifted to the right relative to the low-level waves.

One result of the differential shift in the upper level waves appears to be a consolidation of the upshear rear-to-front and front-to-rear flow and an extended region of upper level outflow on the downshear region of the line (Fig. 6b). The wave contribution to these flow branches is now recognized (on comparing with Fig. 3) as the local maxima and minima θ', u', and π' through the depth of the troposphere on either flank of the line.[3] Because the wave perturbations were smaller within the well-mixed layer, their contribution to the middle-level inflow branches were likewise smaller. This was one factor leading to the disparity in flow strength between the upper and middle-level circulation branches as the system matured.

Second, including vertical wind shear led to a change in the wave magnitude. This was particularly noticeable for the shorter boundary layer waves (compare Figs. 6a and 3a). The favored LRW is the counterpart to the gravity wave without stagnation that formed in the control experiment. The increase in the LRW amplitude was one reason for the resurgence of the long-lived, deep convective-scale updraft in the higher shear cases (Fig. 4).

3) STRONG SHEAR EXPERIMENT (S2)

Recall that the flow used to initialize the model in experiment S2 was designed to replicate the magnitude of the shear in the control experiment and observed in the actual case study. Doubling the shear has led to a further consolidation and strengthening of the upshear rear-to-front and front-to-rear flow and an even higher amplitude in the LRW. These features, which also

[3] We define the line position here as the location of the LRW.

characterize the flow obtained in the control experiment, now appear (comparing Figs. 3, 6, 7) to have been strongly modified by the shear-induced changes in the upper and lower tropospheric wave amplitude and phase speed.

The updraft in experiment S2 is seen to penetrate well into the stratosphere with some indication of it having forced a short, nonhydrostatic lee wave there. Upshear from the updraft, the pressure field becomes hydrostatic with a large high centered near the tropopause between two broad and flattened layers of lower stratospheric cooling and upper tropospheric warming. Similar layers are also evident in experiments S0 and S1 but their dynamics remain somewhat of a mystery. In any event, both layers extend beyond the trailing cirrus cloud shield to the location of the ULW where the isentropes are first seen to diverge from their initial levels. Assuming the flow at this point is approximately isentropic, we infer that there is partial blocking of the ambient flow within the upper troposphere well upshear from the convective-scale updraft (Fig. 7b). Also note that as the isentropes in the upper troposphere are displaced downward, the mixed layer depth is reduced. The parcels in this layer appear to be channeled and accelerate forming the middle-level rear-to-front flow.

A comparison of Figs. 3, 6, and 7 also shows that the surface wind perturbations associated with the LRW increase from 10 m s^{-1} (experiment S0) to 22 m s^{-1} (experiment S2). By four hours (not shown), the surface u' values in S2 approach 34 m s^{-1} (subtract 10 m s^{-1} to obtain ground-relative flow). Though this is quite strong, the modeled surface winds are still less than the observed surface gusts, which were in excess of 30 m s^{-1}.

The increased surface flow in S2 may be attributed to a further rise in the surface pressure due to diabatic cooling and loading associated with the precipitation process. The increase in flow by four hours is just sufficient to form a closed circulation with respect to the wave movement. As suggested by Crook and Moncrieff (1988), this represents a transition from a gravity wave

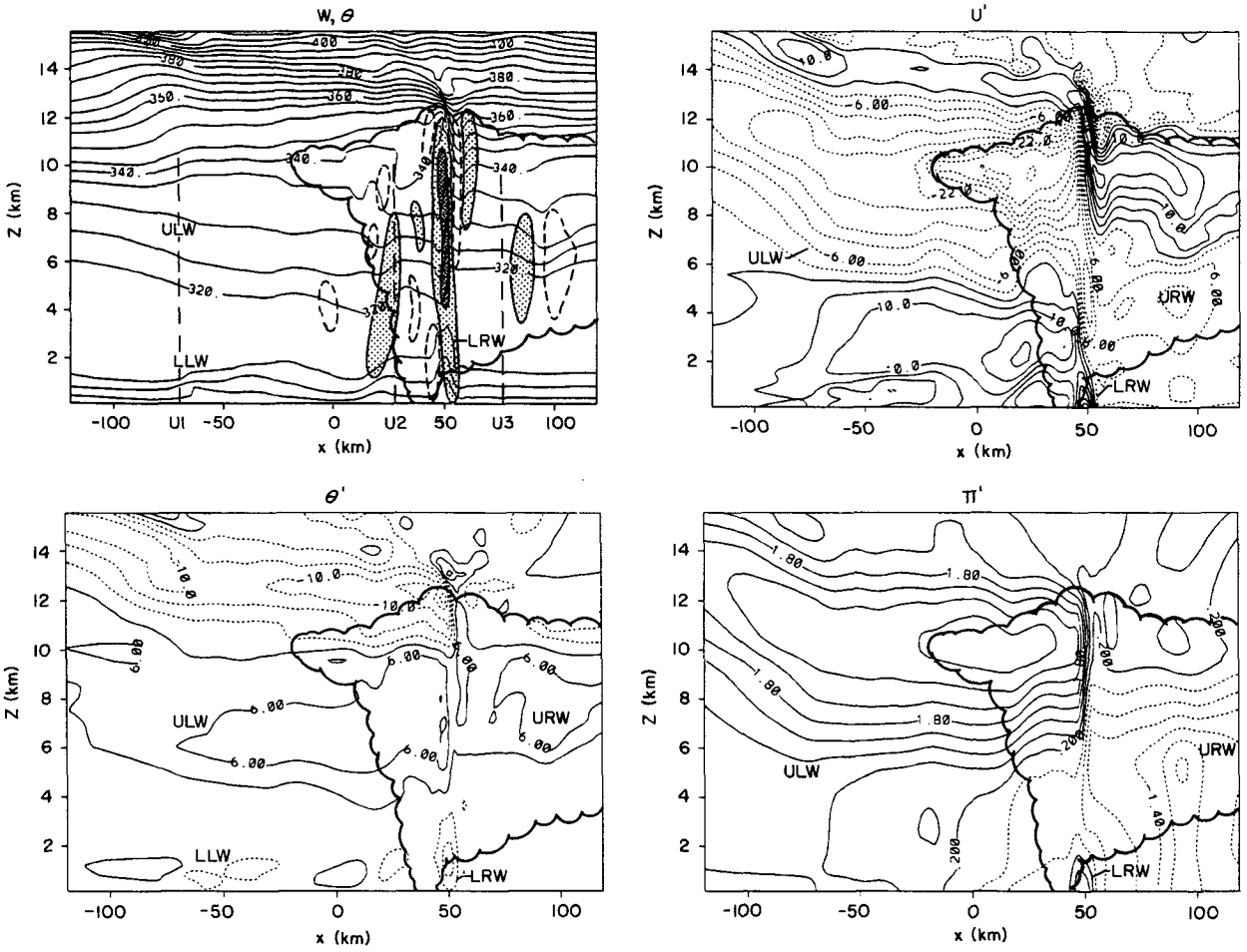

FIG. 7. As in Fig. 6 except for experiment S2 (strong shear) at 7200 s. Note that the contour interval in (c) is 4°C and in (d) 0.4 J kg^{-1} K^{-1}. Dashed vertical lines labeled U1, U2, and U3 in (a) denote the location of the vertical profiles of storm relative u-component shown in Fig. 11.

without stagnation to a gravity wave with stagnation. We infer from a these considerations that a mature density current has yet to develop in the simulation. The squall line propagation during the first four hours is thus a result of wave propagation within the stable ABL. This concept, which appears to date back to Hamilton and Archbold (1945), represents a potentially significant difference in squall line propagation characteristics when a stable, rather than neutral, ABL is present. The issues of how the wave transforms to a density current, and how the density current subsequently interacts with the stable ABL (cf. Raymond and Rotunno 1989), are outside the scope of this paper, but represent some of the fascinating complications to the problem of convective propagation that may occur when a stable layer exists near the surface in a sheared environment.

4) LOW-LEVEL SHEAR (S3)

Confining the vertical shear to the lower levels reproduces the lower-level wave structure of experiment S2, but not the upper-level wave structure (Fig. 8). The upper level waves in this case still experience a slight Doppler shift but the other characteristics evident in Fig. 7, such as the strength of the rear-to-front flow and the vertical displacement of the isentropes, are not as significant. Evidently, these characteristics reflect the sensitivity of the simulation to the interaction between the ULW and the vertical shear profile within the upper troposphere and lower stratosphere.

5) SENSITIVITY TO HORIZONTAL RESOLUTION (FS2)

To test the sensitivity of the simulated flows to horizontal resolution, we reran experiment S2 with a 1 km grid spacing. The results shown in Fig. 9 indicate very few differences in overall structure compared to the run with the coarser resolution. One primary difference was in the strength of the convective-scale updraft (Fig. 4). This was the strongest updraft obtained in any simulation and clearly shows the ability of the line to sustain itself even when the ABL is absolutely stable.

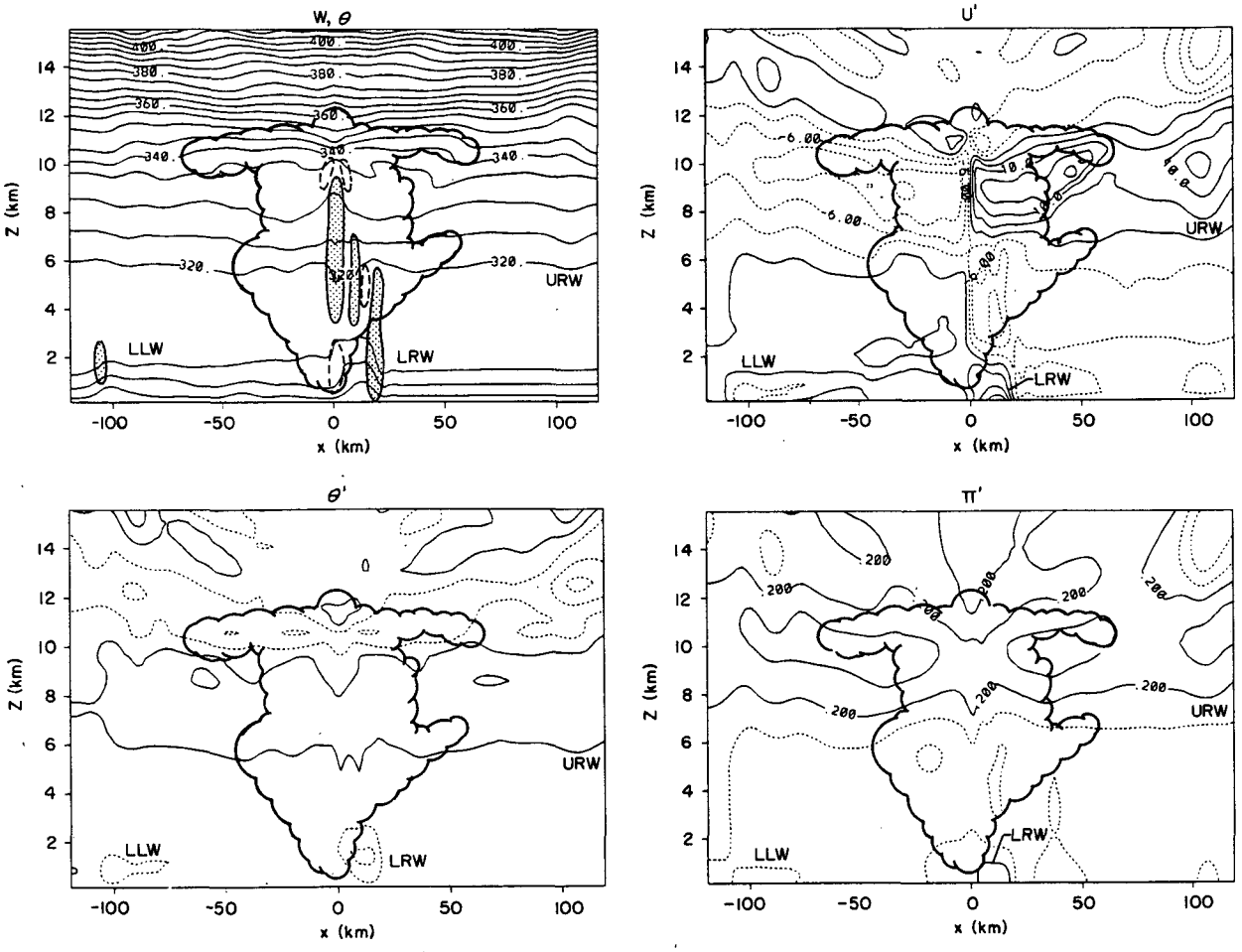

FIG. 8. As in Fig. 7 except for experiment S3 (low-level shear) at 5400 s.

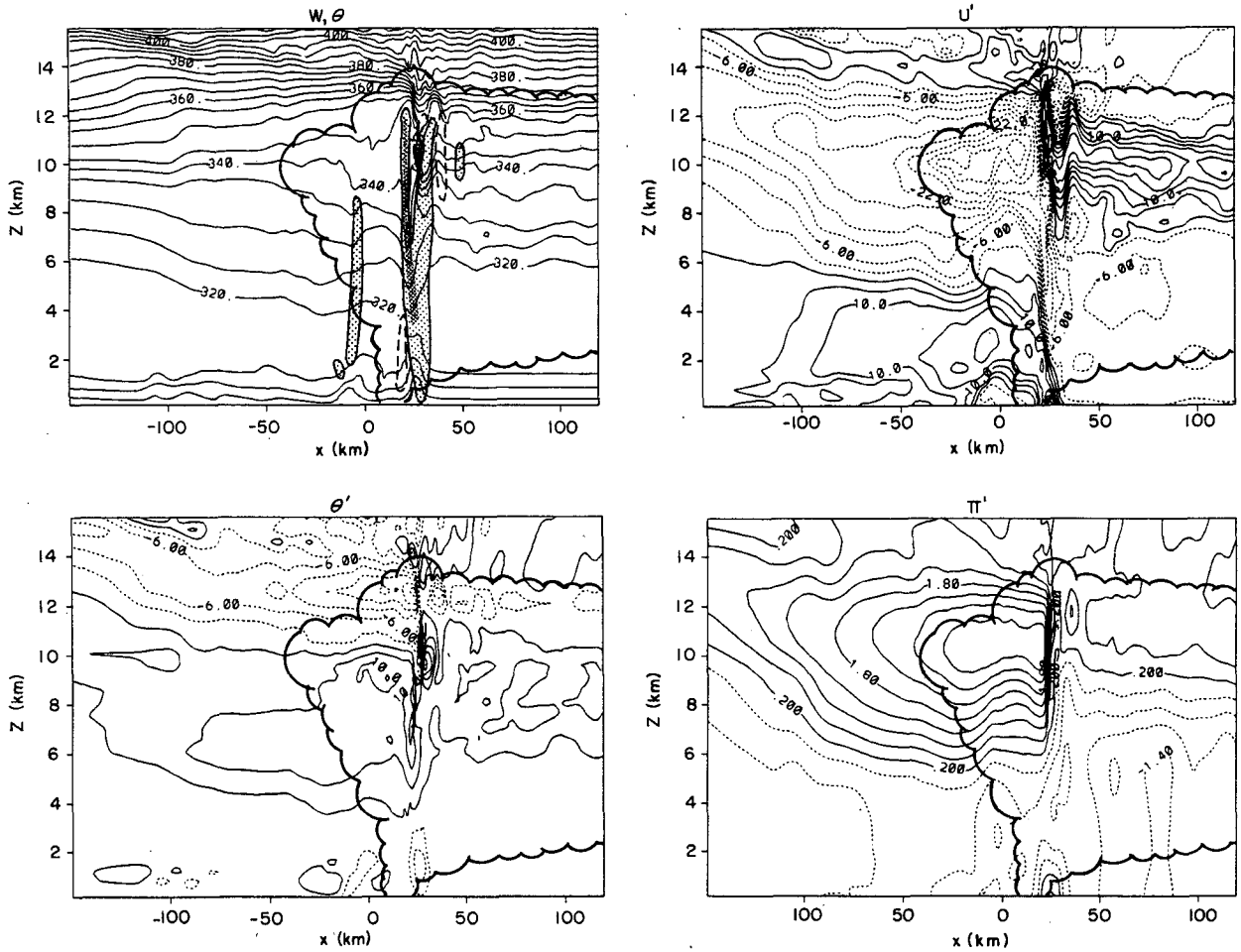

FIG. 9. The results of running experiment S2 with a 1 km horizontal resolution (7200 s). Fields are contoured as in Fig. 7.

c. *Summary of experiments S0–S3*

The model response to the initial heat source in experiments S0–S3 may be summarized as follows. When the simulation is initialized without flow (S0), long-lived gravity waves are generated within the upper and lower troposphere that radiate outward from the initial heat source thereby decreasing its strength (Fig. 10a). The waves excited in each layer differed in horizontal wavelength, magnitude, and phase speed but were otherwise symmetric about a vertical axis through the initial heat source. Once vertical wind shear is introduced, asymmetries develop as the waves experience a Doppler shift in phase speed and a change in magnitude (Fig. 10b,c). The result is a consolidation of the upshear rear-to-front and front-to-rear flow, and reemergence of the deep convective-scale updraft. Increasing the vertical shear aloft led to a vertical displacement of the isentropes over a broad region of the upper troposphere and lower stratosphere on the upshear flank of the line. This led to a partial blocking of the ambient flow within the upper troposphere and a channeling of the flow within the well-mixed layer. In all cases, the line propagation during the first four hours of simulation was a result of wave propagation in the stable ABL.

4. Discussion

We find the relationship between the wave structure and squall line flow fields presented here both interesting and troubling—interesting because the waves appear to exert a strong influence on the 2-D flow fields and troubling because the final results can be directly traced to the initial perturbation. Both results depend, of course, on the longevity of the initial waves, the difference in scale selection between the upper and lower level waves, and the wave interaction with the vertical wind shear. It is these characteristics which are of interest here because they reflect the choice of thermodynamic and shear profiles used in the model, and may thus represent the behavior of waves excited by actual penetrating convective clouds in similar environments.

Unfortunately the simulated wave behavior is difficult to resolve fully here because the waves become nonlinear, and because they quickly alter the ambient

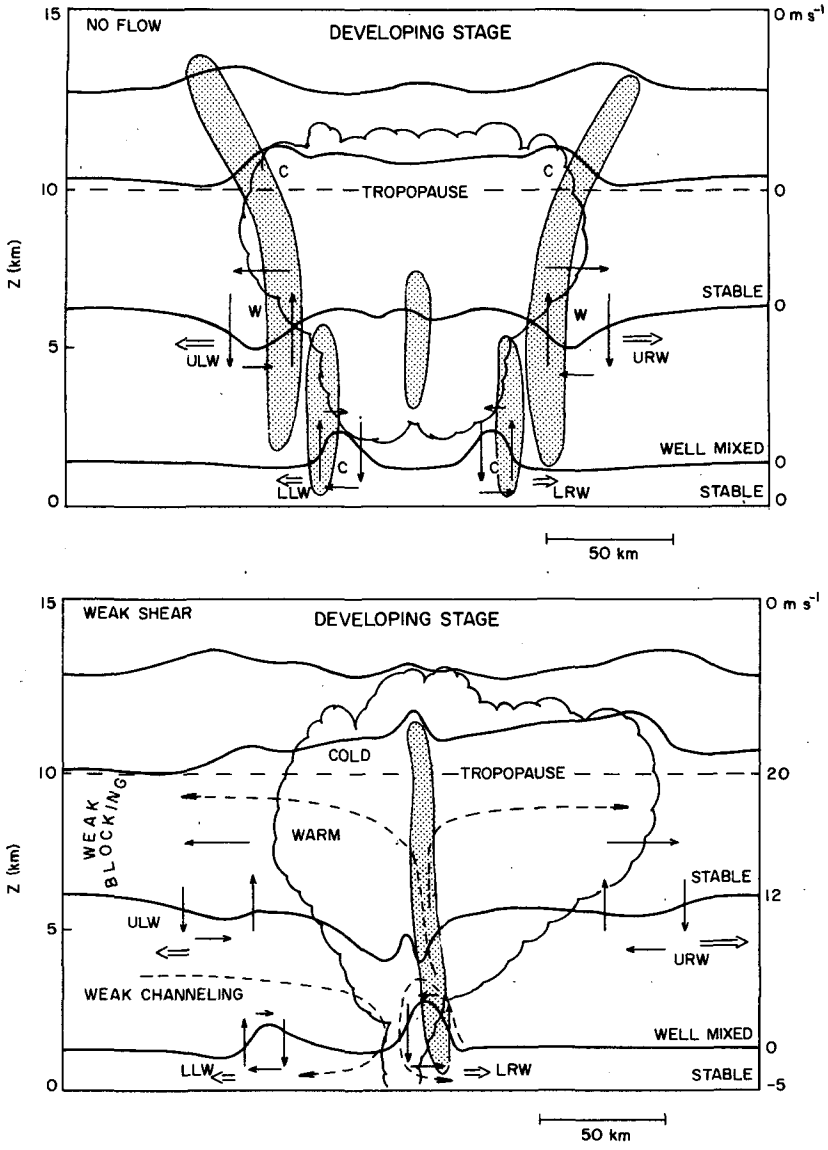

FIG. 10. Conceptual diagram summarizing: (a) experiment S0 (no shear), (b) experiment S1 (weak shear), and (c) experiment S2 (strong shear). The solid lines represent θ surfaces associated with primary waves discussed in the text. The labels C/W in (a) represent, respectively, regions of cold/warm perturbations in θ. Double arrows represent wave movement. Thin arrows denote perturbations in $\dot{w}$ and u. The primary updraft zones are shaded. The numerical values on the right figure boundary refer to the ambient horizontal wind speed in meters per second. Schematic streamlines in (b,c) are meant to suggest the flow resulting from the primary wave modes.

thermodynamic and vertical wind shear profiles through a large region of the domain. These factors hinder a quantitative treatment of the wave behavior using such standard tools as the Taylor–Goldstein equation because the underlying assumptions used in the derivation of this equation are ultimately violated. Provided the waves do not break, however, this equation may still be used to determine, at least qualitatively, some aspects of the simulated wave characteristics. We therefore apply this equation at the beginning of this section to the problems of horizontal scale selection and wave longevity for the primary waves evident in the simplified environment of experiment S0. The wave amplitudes in this experiment were relatively low and the Taylor–Goldstein equation should produce good results. We then discuss changes in the wave structure that arise when vertical wind shear is included and address how the wave/shear interaction may have favored the development of the vigorous line simulated in experiment S2. This second topic also leads to a discussion of a wave-induced mechanism for the wake low and rear inflow jet.

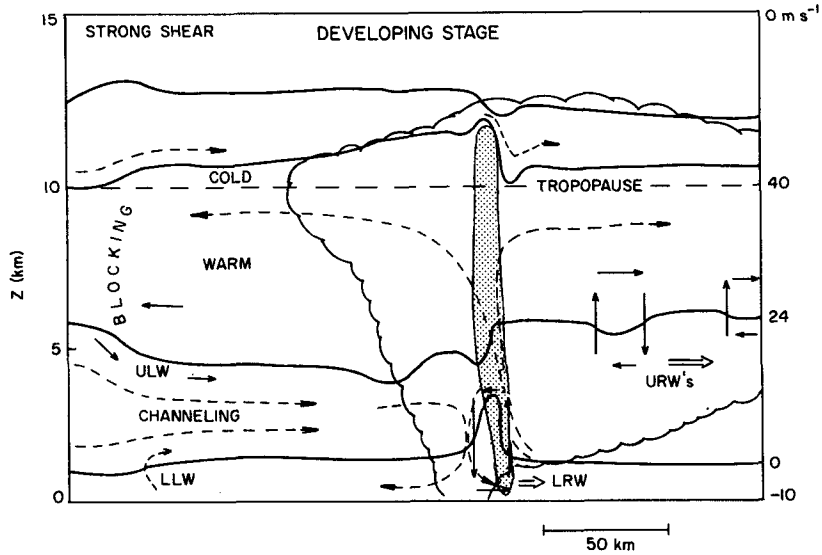

FIG. 10. (*Continued*)

a. Wave longevity and scale selection

The long lifetime of the simulated waves in experiment S0 suggests the horizontal wavelengths were confined such as to minimize the vertical propagation of the wave energy. The trapping conditions for linear waves can be described using the Boussinesq form of the Taylor–Goldstein equation, viz.

$$d^2w/dz^2 + m^2w = 0 \qquad (1)$$

where in the case of linear ambient shear

$$m^2 = N^2/(U(z) - c)^2 - k^2 \quad \text{or} \quad m^2 = l^2 - k^2, \qquad (2)$$

with l^2 being the Scorer parameter, N the Brunt–Väisälä frequency, k the horizontal wavenumber, $U(z)$ the vertical structure of the horizontal flow, and $U(z) - c$ the Doppler shifted phase speed of the wave. If $l^2 < k^2$ above a given level in the atmosphere, the waves become evanescent with height and considerable wave energy may be retained near the source level of the wave (cf. Eliassen and Palm 1961). We see from (2) that this condition is likely met, for a given k, in a layer of low static stability (small N) or in a sheared environment where the values of $U(z) - c$ become large.

The case of initial interest here is one of vertical wave propagation within the lower layer and evanescent behavior within the well-mixed layer. Using typical values of the phase speed for the lower-level waves in the experiment S0 [$U(z) = 0$, $c = \pm 15$ m s^{-1}] and the value of N_2 from Table 1, we find, using (2), that the horizontal wavelength, λ_x, is constrained to 9 km $< \lambda_x <$ 28 km. We see from Fig. 3 that the dominant lower level waves fall within this range and therefore should be long lived. Because the well-mixed layer is relatively shallow, however, the reflection from the upper layer is not complete and some energy tunnels through to the upper stable layer. For the wave to be evanescent in both layers, the horizontal wavelength should be on the order of 10 km. This places a much stronger constraint on those wavelengths in the lower troposphere which are likely to retain significant energy and may partially explain (since nonlinearities might also affect the scale selection) the rather short horizontal wavelength for the simulated lower modes.

The selection of a particular horizontal scale for the upper level waves is less clear. Part of the problem is that the initial long waves excited in the upper layer, though possibly trapped below, are free to propagate vertically into the stratosphere where the values of N are initially much greater. In the shear experiments, one may argue that the strong cooling just at the tropopause level (Fig. 7c) may act to trap subsequent wave energy (cf. Tripoli and Cotton 1989) but this does not suggest a mechanism for the wavelength of the initial waves evident in S0.

Though we presently know of no method to account for the horizontal wavelength in such cases, we are able to suggest a reason for the difference in phase speed between the waves within the upper and lower layers. The wave energy in each layer, trapped or otherwise, will most likely be concentrated in those modes which fit a quarter of a vertical wavelength within the layer and hence experience the greatest resonance between the incident and reflected waves (Gill 1982). The phase speed for the gravest mode in such cases is given by

$$c = \frac{2NH}{\pi} \qquad (3)$$

where H is the depth of the layer. For the lower layer, H is 1500 m, $N_1 = 1.6 \times 10^{-2}$ s^{-1} giving a phase speed

of $c = 16$ m s^{-1}, while for the upper layer, H is 4000 m, $N_3 = 1.0 \times 10^{-2}$ s^{-1} and $c = 29$ m s^{-1}. Both values closely match the simulated phase speed for the upper and lower waves in experiment S0. This suggests that wave resonance in the upper and lower layers could result in a 2-to-1 differential in phase speed.

Even in this simple experiment, though, the final scale selection and wave phase speed may ultimately be governed by nonlinearities. The lower-level waves, in particular, resemble the nonlinear solitary waves discussed by numerous authors (cf. Christie et al. 1978). In such cases, the wave longevity may result from a balance between nonlinear advection, which acts to steepen the wave, and dissipation, which tends to reduce the wave amplitude. Several other complications arise that affect the wave amplitude when vertical wind shear is included. We address some of these issues in the following section.

b. *Wave/shear interaction*

1) UPPER LEVEL WAVES

A distinguishing aspect of these simulations was the tendency for the strongest convection to persist in the environment characterized by the deepest and strongest vertical wind shear. Strong ambient flow generally presents a problem in 2-D models since the air flows through, rather than around, the convective towers. This can lead to a downshear tilt in the updraft within the upper troposphere and the eventual demise of the storm (Hane 1973).

For a storm to overcome this effect, it must develop an opposing flow branch, such as the upper-level front-to-rear flow, that acts to partially block the upper level flow. One source for the upper level outflow is the horizontal mass flux divergence associated with the slowing of convective-scale updraft within the upper troposphere and lower stratosphere. Another source, apparently superimposed on the former, is a result of gravity waves such as the ULW that rapidly move outward from the convective system. It appears that, as the strength of the ambient flow varies aloft, the leading edge of the upper level outflow may result from either a wave, pure mass divergence from the convective-scale updraft, or some combination of the two.

As the flow increased aloft in the various experiments, the upstream progress of the ULW was slowed and its structure appeared to gradually change. These changes had two important effects on the simulation. First, slowing the wave kept it in the near field of the convective line for a longer period of time. Since the circulation about the ULW opposed the environmental shear, it may have acted to buffer the updraft from the debilitating effects of the upper level ambient flow.

The change in vertical shear is shown graphically in Fig. 11. Profile U1 shows the initial reduction in the vertical shear near the ULW. Further reduction occurs near the convective line (profile U2) where we expect the horizontal mass flux divergence to be greater. The U1 and U2 profiles both show strong vertical shear below 3 km, very little shear between 3 and 6 km, and negative vertical shear above 6 km. The U3 profile shows little change below 6 km but a strong increase above this level. The locally modified vertical wind shear profile experienced by the updraft through the lower troposphere thus bears some resemblance to the profiles used successfully in other two-dimensional squall line simulations; i.e., strong low-level shear with reduced shear aloft (cf. Thorpe et al. 1982; Rotunno et al. 1988). The wave-induced reduction in the upper level shear on the upshear flank of the line, coupled with slower wave separation speed from the line, are two factors that may have ultimately aided the development of the long-lived line in these simulations.

Second, structural changes in the ULW occur in the strong shear cases that extend the blocking upshear even as the ULW loses ground to the convective-scale updraft. This can be seen by comparing the structure of the isentropic surfaces in Figs. 3, 7, and 8. In each experiment, there is a tendency for the isentropes to

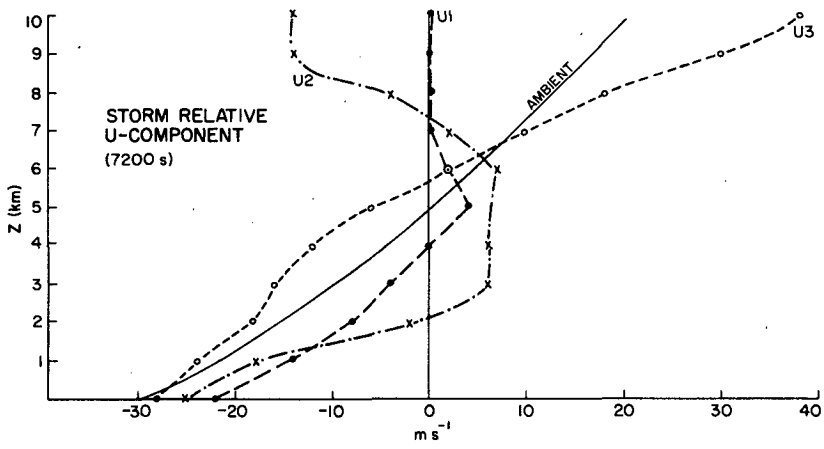

FIG. 11. Vertical profiles of storm-relative u-component for experiment S2. The location of the profiles labeled U1, U2, and U3 are shown in Fig. 7a.

be vertically displaced from their initial levels as the wave passes. As the vertical shear increases aloft, however, the displacement becomes greater and more permanent. The shape of isentropic surfaces in Fig. 7a suggests a hydraulic jump may be forming as the local Froude number (U/NH) increases and the flow becomes supercritical with respect to the ULW. As we show in the following section, the displacement not only extends the upper level blocking upshear in the strong shear cases but also affects the development of the rear-to-front jet located within the lower troposphere.

2) A MECHANISM FOR THE FORMATION OF THE WAKE LOW AND REAR IN-FLOW JET

One of the dominant features in many squall lines is the middle-level, rear-to-front jet. The jet in our case is shown in Fig. 12 along with the fields of u' and π' for experiment S2. We see from this figure that the jet axis is centered slightly above the axis of maximum u' within the middle troposphere and makes a rather abrupt jump upward toward the tropopause level near the location of the ULW.

It is somewhat easier to understand how the jet forms in this simulation by looking at the development of the u' field. To begin, recall that a deep, cold layer progressed rapidly upshear within the lower stratosphere (Fig. 7c) forming a large high pressure region centered near the tropopause (Fig. 7d). Consider the effects of this pressure perturbation on a parcel within the upper troposphere as it approaches the system in the upper level westerly flow. A parcel moving toward the right near point A (Fig. 12) experiences a downward directed pressure gradient force and begins to sink creating positive θ'. Sinking is enhanced near the position of the ULW (point B) and continues until the parcel's newly acquired buoyancy opposes the pressure field generated by the cold air aloft (point C). Further lifting or sinking of the parcel after this point then depends on the structure the overlying cold air or diabatic effects as the parcel nears or enters the trailing cirrus cloud shield.

The amount of warming (or vertical displacement) can be estimated assuming the final adjustment is in hydrostatic balance. The perturbation hydrostatic equation in terms of the Exner function has the following form:

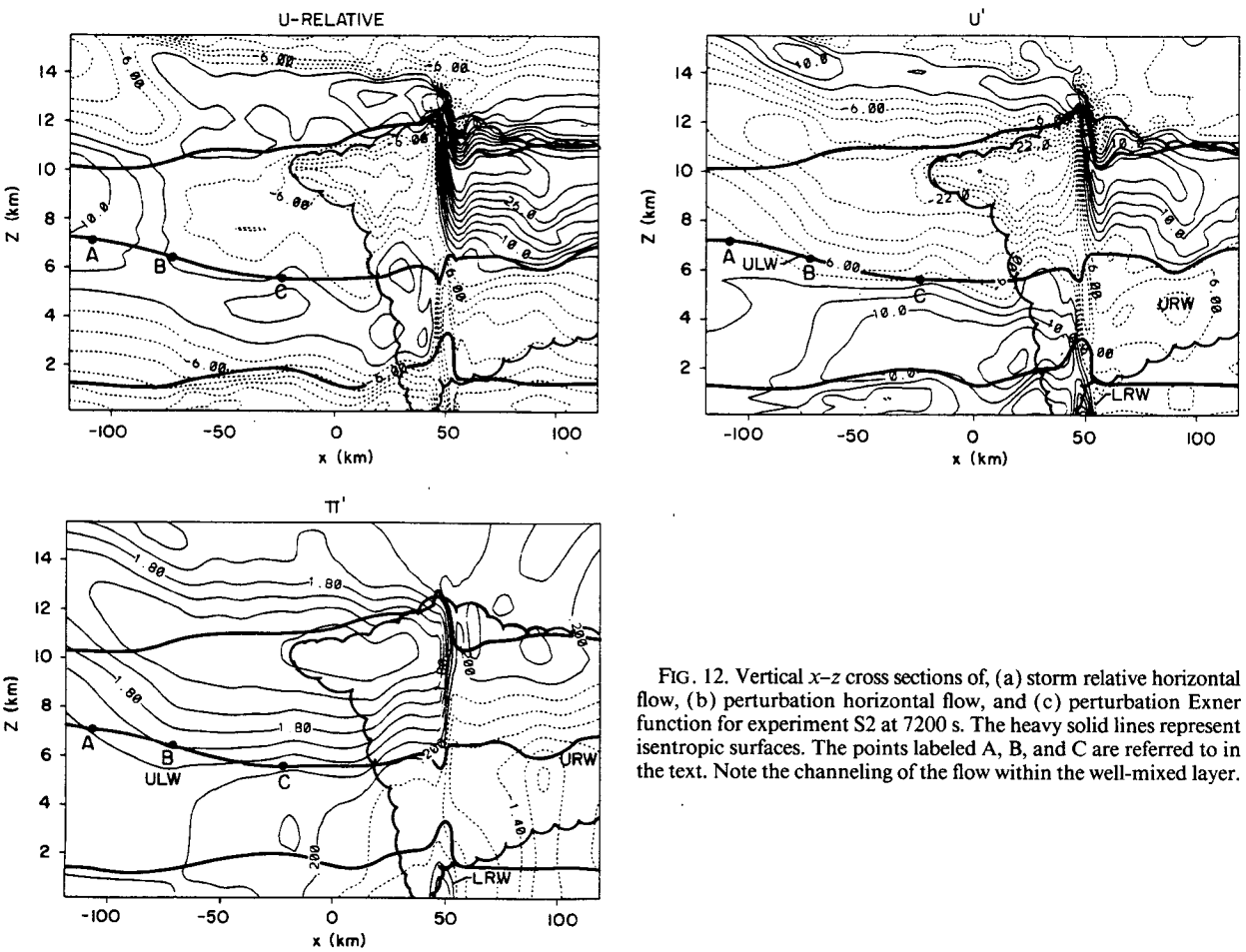

FIG. 12. Vertical x–z cross sections of, (a) storm relative horizontal flow, (b) perturbation horizontal flow, and (c) perturbation Exner function for experiment S2 at 7200 s. The heavy solid lines represent isentropic surfaces. The points labeled A, B, and C are referred to in the text. Note the channeling of the flow within the well-mixed layer.

$$\frac{\partial \pi'}{\partial z} = \frac{g\theta'}{\theta_0{}^2}. \tag{4}$$

Using representative values of π' and θ_0 from Fig. 7, we estimate from (4) a mean θ' value of

$$\frac{1.8 \text{ J kg}^{-1} \text{ K}^{-1} \, 330^2 \text{ K}^2}{4000 \text{ m } 9.8 \text{ m s}^{-2}} = \theta' = 5 \text{ K}.$$

This is in good agreement with the mean value of θ' within a broad region of the upper troposphere on the upshear portion of the line (Fig. 7c). Based on the environmental sounding, one can estimate that parcels in the upper troposphere must sink approximately 1500 m to produce the θ' required for hydrostatic balance. This corresponds well with the deflection of the θ surfaces evident in Fig. 7a.

One effect of the displacement is to create a net change in the thickness of the middle-level well-mixed layer (Fig. 7a). A comparison to the mixed layer depth far upshear suggests that the flow is channeled in this layer (see Figs. 7a,b). We therefore expect an acceleration of the flow (Fig. 7b) and, through a Bernoulli-like effect, a lowering of the pressure (Fig. 7d). Similar reasoning was used by Parsons et al. (1988) to explain the observed pressure lowering over surface cold pools. Note that the channeling should be enhanced in this case because the surface layer is initially stable. For other systems, the channeling would increase as the cold surface mesohigh develops. The combination of pressure lowering from subsidence warming, which is maximized beneath the ULW, and subsequent parcel acceleration within the jet, may be a reason for the correlation between the wake low/rear inflow jet that occurs in many observed squall line systems (cf. Johnson and Hamilton 1989).

3) LOW-LEVEL WAVES

The advantages to the convective-scale updraft, resulting from a reduction in the vertical wind shear aloft, are somewhat offset by the large region of warming that arises in the upper troposphere. The warming should weaken the updraft due to a reduction in the local buoyancy. There are two factors that oppose this effect. First, the overlying layer of cold air in the lower stratosphere abruptly ends just above the updraft as the lee wave forms (Figs. 7a,c). The parcels within the upper troposphere, sensing a reduction in the upper level pressure field that initially forced them to sink, are then able to rise just as abruptly (see the isentropic surfaces near the convective-scaled updraft in Fig. 7a). Thus there may be a contribution to the convective-scale (and perhaps the mesoscale updraft) as parcels rebound from dynamically induced subsidence well upshear from the line.

One additional factor aiding the maintenance of the updraft in the strong shear cases was the increased low-level lift that developed as the LRW increased in amplitude. Though this was an important aspect of the simulation, it is one we do not yet fully understand. We list below a few of many factors that may have influenced the wave amplification but further study is required to clarify the exact mechanism. The low-level wave amplitude increase in the sheared environments may have been affected by: 1) an increase in the mean flow, which may have advected energy released in the convective-scale updraft at the speed of the low-level ducted wave, thereby leading to possible growth of the wave (Raymond 1986); 2) critical level encounters and possible wave resonance (Clark and Peltier 1984); 3) differential horizontal advection which, because it affects the wave trough and peaks differently, may either steepen or flatten the wave; and 4) an imbalance between the horizontal vorticity of the wave and the horizontal vorticity of the environmental wind shear. This last process has been shown by Rotunno et al. (1988) to affect the slope of the vertical motion field. In our case, this may change the shape of the wave.

5. Summary and conclusions

A two-dimensional version of the CSU RAMS, initialized with a simplified thermodynamic structure and variable vertical wind shear, was used to show the role of internal gravity waves in modifying the behavior and structure of a simulated squall line. The waves were generated as a warm bubble, used to initialize the experiments, accelerated upward through a three-layered troposphere comprised of two stable layers separated by a deep well-mixed layer. This thermodynamic profile, though derived from a convectively modified environment, may also be characteristic of nocturnal or frontal squall lines. The mixed layer provided sufficient instability to sustain deep convective updrafts and was proficient at trapping wave energy generated in the surrounding stable layers. The waves were thus long lived and had a significant impact on the simulated flow fields.

In these experiments, we fixed the depth of the various layers within the troposphere and tested for a sensitivity to changes in the vertical wind shear profiles. An experiment initialized without flow (S0), produced a field of gravity waves in the upper and lower stable layers that had left/right symmetry about a vertical axis through the initial heat source. The waves accounted for the broad structural similarities with the horizontal flow fields obtained for the control squall line (generated by an observed sounding). The upper and lower tropospheric waves differed in horizontal wavelength, phase speed, and magnitude, however, and this quickly lead to asymmetries in the modeled flow fields once vertical shear was introduced in the model.

With vertical wind shear, the upper and lower tropospheric waves experienced a Doppler shift in phase speed and a change in magnitude. The change in wave magnitude was most noticeable in the lower stable layer as a high amplitude gravity wave with stagnation developed. This wave determined the propagation speed

of the squall line and was instrumental in lifting the low-level air to the level of free convection. This suggests that the wave dynamics may play an important role in the propagation of squall lines when the ABL is stable. The ABL wave was also associated with surface wind perturbations of 34 m s^{-1}. Such strong perturbations in a stable environment are characteristic of derechos (Johns and Hirt 1987). The results presented here suggests these systems may be influenced by growing waves within the stable ABL.

The simulations were also sensitive to the vertical wind shear within the upper troposphere and lower stratosphere. As the shear increased aloft, the isentropes within the upper troposphere on the upshear flank of the line became displaced from their initial levels over a broad region. This led to a partial blocking of the flow aloft and a channeling of the flow below. The blocking reduced the upper-level vertical wind shear experienced by the updraft. The channeling led to the development of the rear-to-front jet within the middle-level, well-mixed layer. The channeling was enhanced beneath the ULW as the isentropes abruptly lowered to their new levels. This was also the region where the upper-level subsidence was a maximum. The pressure reduction from subsidence warming and horizontal acceleration of the flow may be a reason for the correlation between the wake low and rear inflow jet that often accompany squall line systems.

The significance of the gravity waves discussed above is magnified by the two dimensionality imposed on the simulations. Furthermore, nonlinear processes are likely important and, consequently, the application of linear wave theory used to describe their behavior is an oversimplification. We are also troubled that the evolution of the perturbed fields was so closely tied to the waves induced by the initial perturbation. This may point to a problem using a warm bubble initialization when the thermodynamic environment naturally supports long-lived waves. We believe, however, that similar wave behavior will also be induced by natural cloud forming processes. Any explosive convective development will generate gravity waves that may then alter the local vertical wind shear and thermodynamic profiles within the troposphere. We have tried to address how these interactions arose in a particular environment and how they may have effected the simulated storm. It cannot be overlooked that the simulations were also sensitive to the profiles of vertical wind shear and stability profiles within the lower stratosphere.

Acknowledgments. The authors benefited from discussions with Dr. Duane Stevens, Dr. Melvin Nicholls, Mike Weissbluth, James Bossert, and Ray McAnelly. Craig Tremback and Dr. Robert Walko are acknowledged for their advice concerning the use of the CSU RAMS. Brenda Thompson is also acknowledged for her help in preparing the manuscript. This research was supported by the National Science Foundation under Grant ATM-8814913. The computations were performed on the NCAR CRAY computing system. NCAR is supported by the National Science Foundation.

REFERENCES

Abdullah, A. J. 1954: The meridional growth of squall lines. *J. Meteor.*, **11**, 301–308.

Balaji, V., and T. L. Clark, 1988: Scale selection in locally forced convective fields and the initiation of deep cumulus. *J. Atmos. Sci.* **45**, 3188–3211.

Benjamin, S. G., and T. B. Carlson, 1986: Some effects of surface heating and topography on the regional severe storm environment. Part I: Three-dimensional simulations. *Mon. Wea. Rev.*, **114**, 307–329.

Bolton, D., 1984: Generation and propagation of African squall lines. *Quart. J. Ray. Meteor. Soc.*, **110**, 695–721.

Bosart, L. F., and A. Seimon, 1988: A case study of an unusually intense atmospheric gravity wave. *Mon. Wea. Rev.*, **116**, 1857–1886.

Branick, M. L., F. Vitale, C. Lai and L. F. Bosart, 1988: The synoptic and subsynoptic structure of a long-lived severe convective system. *Mon. Wea. Rev.*, **116**, 1335–1370.

Brunk, I. W., 1949: The pressure pulsation of 11 April, 1944. *J. Meteor.*, **6**, 395–401.

Carbone, R. E., 1982: A severe frontal rainband. Part I: Stormwide hydrodynamic structure. *J. Atmos. Sci.* **39**, 258–279.

Carr, F. H., and J. P. Millard, 1985: A composite of comma clouds and their association with severe weather over the Great Plains. *Mon. Wea. Rev.*, **113**, 370–387.

Christie, D. R., K. J. Muirhead and A. L. Hales, 1978: On solitary waves in the atmosphere. *J. Atmos. Sci.*, **35**, 805–825.

Clark, T. L., and W. R. Peltier, 1984: Critical level reflection and the resonant growth of nonlinear mountain waves. *J. Atmos. Sci.*, **41**, 3122–3134.

Crook, N. A., and M. W. Moncrieff, 1988: The effect of large-scale convergence on the generation and maintenance of deep moist convection. *J. Atmos. Sci.*, **45**, 3606–3624.

Dudhia, J., M. W. Moncrieff and D. W. K. So, 1987: The two-dimensional dynamics of West African squall lines. *Quart. J. Roy. Meteor. Soc.*, **113**, 121–146.

Eliassen, A., and E. Palm, 1961: On the transfer of energy in stationary mountain waves. *Geofys. Publ.*, **22**, 1–23.

Emanuel, K. A., 1982: Inertial instability and mesoscale convective systems. Part II: Symmetric CISK in a baroclinic flow. *J. Atmos. Sci.*, **39**, 1080–1097.

Eom, J., 1975: Analysis of the internal gravity wave occurrence of 19 April 1970 in the Midwest. *Mon. Wea. Rev.*, **103**, 217–226.

Freeman, J. C., 1948: An analogy between the equatorial easterlies and supersonic gas flows. *J. Meteor.*, **5**, 138–146.

Fulks, J. R., 1951: The instability line. *Compendium Meteorology*, Amer. Meteor. Soc., 6 pp.

Gill, A. E., Atmosphere–Ocean Dynamics. Academic Press, 1982.

Hamilton, R. A., and J. W. Archbold, 1945: Meteorology of Nigeria and adjacent territory. *Quart. J. Roy. Meteor.*, **71**, 231–264.

Hane, C. E., 1973: The squall line thunderstorm: Numerical experimentation. *J. Atmos. Sci.*, **30**, 1672–1690.

Johns, R. H., and W. D. Hirt, 1987: Derechos: Widespread convectively induced windstorms. *Wea. Forecasting*, **2**, 32–49.

Klemp, J. B., and R. B. Wilhelmson, 1978a: The simulation of three-dimensional convective storm dynamics. *J. Atmos. Sci.*, **35**, 1070–1096.

——, and ——, 1978b: Simulations of right- and left-moving storms produced through storm splitting. *J. Atmos. Sci.* **35**, 1097–1110.

Koch, S. E., R. E. Golus and B. Dorian, 1988: A mesoscale gravity wave event observed during CCOPE. Part II: Interaction between mesoscale convective systems and the antecedent waves. *Mon. Wea. Rev.* **116**, 2545–2569.

Lin, Y. L., and R. B. Smith, 1986: Transient dynamics of airflow near a local heat source. *J. Atmos. Sci.*, **43**, 40–49.

——, and S. Li, 1988: Three-dimensional response of shear flow to elevated heating. *J. Atmos. Sci.*, **45**, 2987–3002.

Lindzen, R. S., and K. K. Tung, 1976: Banded convective activity and ducted gravity waves. *Mon. Wea. Rev.*, **104**, 1602–1617.

Miller, D. A., and F. Sanders, 1980: Mesoscale conditions for the severe conditions of 3 April 1974 in the east-central United States. *J. Atmos. Sci.*, **37**, 1041–1055.

Miller, L. J., J. D. Tuttle and C. A. Knight, 1988: Airflow and hail growth in a severe northern High Plains supercell. *J. Atmos. Sci.*, **45**, 736–762.

Nehrkorn, T., 1986: Wave-CISK in a baroclinic basic state. *J. Atmos. Sci.*, **43**, 2773–2791.

Newton, C. W., 1950: Structure and mechanism of the prefrontal squall line. *J. Meteor.*, **8**, 210–222.

——, 1966: Circulations in large sheared cumulonimbus. *Tellus*, **18**, 699–713.

Nicholls, M. E., 1987: A numerical investigation of tropical squall lines. Ph.D. dissertation, Colorado State University, 174 pp.

——, 1989: Thermally forced gravity waves. Part I: A linear model of mesoscale convective systems. *J. Atmos. Sci.*, submitted.

Orlanski, I., and B. B. Ross, 1986: Low-level updrafts in stable layers forced by convection. *J. Atmos. Sci.*, **43**, 997–1005.

Parsons, D. B., C. G. Mohr and T. Gal-Chen, 1987: A severe frontal rainband. Part III: Derived thermodynamic structure. *J. Atmos. Sci.*, **44**, 1615–1631.

Porter, J. M., L. L. Means, J. E. Hovde and W. B. Chappell, 1955: A synoptic study on the formation of squall lines in the north central United States. *Bull. Amer. Meteor. Soc.*, **36**, 390–396.

Raymond, D. J., 1984: A wave–CISK model of squall lines. *J. Atmos. Sci.*, **41**, 1946–1958.

——, 1986: Prescribed heating of a stratified atmosphere as a model for moist convection. *J. Atmos. Sci.*, **43**, 1101–1111.

——, and R. Rotunno, 1989: Response of a stably stratified flow to cooling. *J. Atmos. Sci.*, **46**, 2830–2837.

Rotunno, R., J. B. Klemp and M. L. Weisman, 1988: A theory for strong, long-lived squall lines. *J. Atmos. Sci.*, **45**,463–485.

Smull, B. F., and R. A. Houze, Jr., 1987: Rear inflow in squall lines with trailing stratiform precipitation. *Mon. Wea. Rev.*, **115**, 2869–2889.

Schmidt, J. M., and W. R. Cotton, 1989: A High Plains squall line associated with severe surface winds. *J. Atmos. Sci.*, **40**, 281–302.

Stobie, J. G., F. Einaudi and L. W. Uccellini, 1983: A case study of gravity waves-convective storms interaction: 9 May 1979. *J. Atmos. Sci.*, **40**, 2804–2830.

Tepper, M., 1950: A proposed mechanism of squall lines: The pressure jump line. *J. Meteor.*, **7**, 21–29.

Thorpe, A. J., M. J. Miller and M. W. Moncrieff, 1982: Two-dimensional convection in non-constant shear: A model of mid-latitude squall lines. *Quart. J. Roy. Meteor. Soc.*, **108**, 739–762.

Tripoli, G. J., 1986: A numerical investigation of an orogenic mesoscale convective system. Ph.D. dissertation, Colorado State University, (atmospheric science paper No. 401). 80523, 290 pp.

——, and W. R. Cotton, 1989a: A numerical study of an observed orogenic mesoscale convective system. Part I: Simulated genesis and comparison with observations, *Mon. Wea. Rev.*, **117**, 269–300.

——, and W. R. Cotton, 1989b: A numerical study of an observed orogenic mesoscale convective system. Part II: Analysis of governing dynamics, *Mon. Wea. Rev.*, **117**, 301–324.

Uccellini, L. W., 1975: A case study of apparent gravity wave initiation of severe convective storms. *Mon. Wea. Rev.*, **103**, 497–513.